Multi-annual ocean-atmosphere adjustments to radiative forcing

Multiannual Ocean–Atmosphere Adjustments to Radiative Forcing

MARIA A. A. RUGENSTEIN

Institute for Atmospheric and Climate Science, ETH Zürich, Zurich, Switzerland

JONATHAN M. GREGORY

National Centre for Atmospheric Science–Climate, Department of Meteorology, University of Reading, Reading, and Met Office, Hadley Centre, Exeter, United Kingdom

NATHALIE SCHALLER, JAN SEDLÁČEK, AND RETO KNUTTI

Institute for Atmospheric and Climate Science, ETH Zürich, Zurich, Switzerland

(Manuscript received and in final form 21 April 2016)

ABSTRACT

In radiative forcing and climate feedback frameworks, the initial stratospheric and tropospheric adjustments to a forcing agent can be treated as part of the forcing and not as a feedback, as long as the average global surface temperature response is negligible. Here, a very large initial condition ensemble of the Community Earth System Model is used to analyze how the ocean shapes the fast response to radiative forcing. It is shown that not only the stratosphere and troposphere but also the ocean adjusts. This oceanic adjustment includes meridional ocean heat transport convergence anomalies, which are locally as large as the surface heat flux anomalies, and an increase of the Atlantic meridional overturning circulation. These oceanic adjustments set the lower boundary condition for the atmospheric response of the first few years, in particular, the shortwave cloud radiative effect. This cloud adjustment causes a nonlinear relationship between global energy imbalance and temperature. It proceeds with a characteristic time scale of a few years in response to the forcing rather than scaling nonlinearly with global mean temperature anomaly. It is proposed that even very short time scales are treated as a fully coupled problem and encourage other modeling groups to investigate whether our description also suits their models' behavior. A definition of the forcing term ("virtual forcing") including oceanic adjustment processes is introduced and serves as an interpretive idea for longer time scales.

1. Introduction and tropospheric adjustment

The response of the global energy budget to an external perturbation of the energy content can be described by the heat uptake of ocean, ice, and land (N), the perturbation or radiative forcing (F), and the feedback response (λT), with the climate feedback parameter λ and temperature anomaly T:

$$C\frac{dT}{dt} = N = F - \lambda T, \tag{1}$$

with the heat capacity of the climate system, C. Changes that are mediated by the climate system's response to the perturbation are called feedback responses. In contrast, changes that depend on the nature of the perturbation, before the global temperature response happens, are termed adjustments. While the differentiation between forcing and feedbacks is seemingly a nominal problem, their clear separation is important to compare global climate models (GCMs), to calibrate models that do not represent radiation and feedbacks dynamically, and to determine the widely used equilibrium climate sensitivity (ECS) from both models and observations (Gregory et al. 2004; Rogelj et al. 2011; Geoffroy et al. 2013a; Long et al. 2013). In this paper, we put forward the idea of multiannual coupled atmosphere–ocean adjustments. We use a large abrupt4×CO_2 ensemble to robustly detect this adjustment and ascribe it to the

Corresponding author address: Maria Rugenstein, IAC, ETH Zürich, Universitätstrasse 16, Zürich, Switzerland.
E-mail: maria.rugenstein@env.ethz.ch

Publisher's Note: This article was revised on 2 August 2016 to correct formatting errors before and after the presentation of Eq. (2a) in section 3.

DOI: 10.1175/JCLI-D-16-0312.1

oceanic response to radiative forcing. We argue with a new conceptual modification of Eq. (1) that these processes are indeed time-dependent adjustments to the forcing and not temperature-dependent feedback responses. We suggest that the use of a modified forcing term—''virtual forcing,'' which includes the multiannual adjustments—is a useful interpretative idea for longer time scales. We now first discuss tropospheric adjustment mechanisms in detail.

In climate models, adjustments in the stratosphere have long been accounted for when determining radiative forcings (Shine et al. 1990). The concept of tropospheric adjustment emerged only recently. Tropospheric effects have been called ''fast feedbacks'' or ''the initial fast features'' (Lahellec and Dufresne 2014), ''semi-direct effects'' (Andrews and Forster 2008), ''fast responses,'' ''rapid adjustments'' (Bala et al. 2010), or ''direct response to CO_2'' (e.g., Merlis 2015). The separation between fast tropospheric adjustments and feedbacks partly arises from the approximation of the global radiative response by a feedback term that depends linearly on global temperature anomaly [λT in Eq. (1)]. Tropospheric adjustments, which have short time scales, are included in the effective radiative forcing (ERF; e.g., Boucher et al. 2014; Forster et al. 2013).

From a process point of view, tropospheric adjustment for CO_2 happens because directly after the forcing is applied, the radiative imbalance at Earth's surface is smaller than at the top of the atmosphere (TOA). The middle and lower troposphere warm before the surface temperatures increase, causing increased stability, and reduced evaporation, convection, and precipitation over oceans (Cao et al. 2012; Andrews et al. 2012; Kamae et al. 2015).The tropical upward velocities weaken over the oceans and strengthen over land in all models (Bony et al. 2013). The circulation also weakens—independently of the land–sea warming contrast—due to the spatial pattern of the CO_2 radiative forcing acting on the climatological distribution of clouds and humidity (Merlis 2015). Trace gases alone force the stratosphere and upper troposphere to increase the eddy momentum flux, to accelerate stratospheric westerlies, and to displace the tropospheric jets poleward without any sea surface temperature response (Wu et al. 2012; Grise and Polvani 2014a; Staten et al. 2014). Either the reduced surface latent heat flux or the reduced relative humidity at the top of the boundary layer leads to a reduction in low-level cloud cover (Colman and McAvaney 2011; Kamae and Watanabe 2013; Wyant et al. 2012; Watanabe et al. 2012; Tomassini et al. 2013; Zelinka et al. 2013). The cloud response can be attributed to both the aforementioned dynamic and thermodynamic component. Other adjustment effects are the increased transport of heat from the land to the ocean due to enhanced land–ocean heating contrast (Williams et al. 2008; Dong et al. 2009; Webb et al. 2013) and the CO_2 physiological effect, which enhances the land warming and moisture transport onto land (Cao et al. 2011; Kravitz et al. 2013; Doutriaux-Boucher et al. 2009; Kamae and Watanabe 2013). Different forcing agents, such as solar or CO_2 forcing, show different adjustment processes (Lambert and Faull 2007; Bala et al. 2010; Andrews et al. 2010; Schaller et al. 2013). Overall, the tropospheric CO_2 adjustment is also defined as the sum of all processes that happen before the net forcing at the TOA and surface are equal, operating as a measure of the equilibration of the troposphere with the surface (Bala et al. 2010; Lahellec and Dufresne 2014).

Some of the tropospheric adjustment effects are consistent across models, while others are model dependent, or even model version or cloud scheme dependent (e.g., Chung and Soden 2015a). Studies disagree as to how important the different tropospheric adjustment processes are compared to long-term or equilibrium responses. Williams et al. (2008), Andrews and Forster (2008), Gregory and Webb (2008), Bala et al. (2010), Webb et al. (2013), Bony et al. (2013), and Lahellec and Dufresne (2014) find that the ECS or the overall uncertainty to external forcing is influenced, whereas Tomassini et al. (2013), Vial et al. (2013), and Grise and Polvani (2014b) find no statistically significant effect of (their) adjustment processes on the feedback strengths or ECS. Ringer et al. (2014) show a correlation between forcing and feedback, which further complicates the distinction between the two and is discussed further in section 5.

There is no a priori reason why all adjustment processes should be fast, so the distinction between adjustment and surface temperature–mediated response is not clear (Williams et al. 2008; Caldeira and Myhrvold 2013; Zelinka et al. 2013; Sherwood et al. 2014). Some forcing-dependent processes may take place over months or years after the imposition of the forcing, during which the temperature may increase by several degrees, so adjustment and feedback may be taking place simultaneously. An adjustment process influences the local temperatures and heat fluxes, but has little impact on the global mean surface temperature [T in Eq. (1)]. We define the system that is being forced and that experiences adjustments and feedbacks as that which determines T.

Technically, the spatial pattern of a tropospheric adjustment response is determined by either fixed sea surface temperature (SST) runs, in which a climatological SST field is prescribed [used, e.g., in Hansen et al. (2005), Bala et al. (2010), Andrews et al. (2012), Zelinka et al. (2013), and Meraner et al. (2013)] by defining the adjustment as the first year of a $4\times CO_2$ simulation of a coupled model [used, e.g., in Kravitz et al. (2013) and

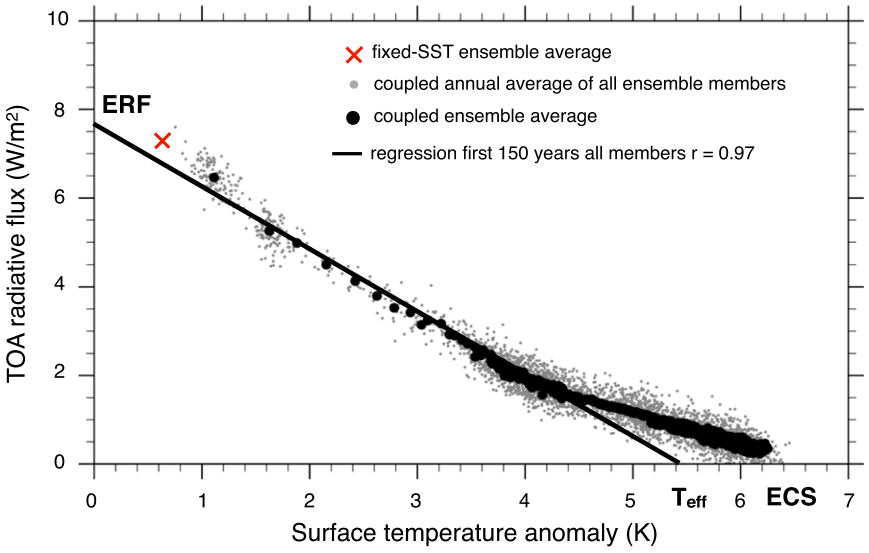

FIG. 1. Global mean net TOA downward radiative flux evolution against global average surface air temperature change of the large abrupt 4×CO_2 ensemble. The regression covers the first 150 yr (black line). Small dots depict the 121 ensemble member annual averages, while large dots are ensemble averages—annual until year 100, at ~4.4-K temperature increase, and decadal afterward.

Bony et al. (2013)] or a slab ocean model [used, e.g., in Bony et al. (2013) and Grise and Polvani (2014b)] or by regressing each grid boxes' variable evolution against the global mean surface air temperature (Gregory and Webb 2008; Andrews et al. 2015). Attempts and problems using radiative kernels to define the tropospheric adjustment response are discussed in Chung and Soden (2015a), Block and Mauritsen (2013), and Larson and Portmann (2015). Forcings are determined by either fixing the global surface temperature (Shine et al. 2003), or—more commonly—fixed-SST simulations, a regression method, which uses Eq. (1) and regresses N, the TOA flux imbalance, against T, the surface temperature response (Fig. 1), or radiative kernels [see Chung and Soden (2015b) for a comparison of the different definitions of radiative forcings].

In this paper, we want to challenge the common understanding of subannual tropospheric adjustment. We find robust multiannual adjustment responses in a large ensemble of coupled simulations introduced in section 2. This response includes mechanisms described above, but we also find the ocean to strongly adjust to the radiative forcing, shaping in turn the tropospheric adjustment processes. We introduce a conceptual framework to show that this response is indeed better described as a time-dependent forcing adjustment than a temperature-dependent feedback (section 3). We then show in the large ensemble that the multiannual adjustment is caused by shortwave cloud radiative effect over the oceans and argue that this is due to the spatial pattern formation of sea surface temperature, ocean heat uptake and loss, and the meridional ocean heat transport (section 4). Finally, since the conventional definitions of radiative forcing only include the adjustment of subannual tropospheric processes, we discuss the consequences of oceanic adjustment for the definition of radiative forcing (section 5).

2. Model and experimental setup

We generate a large initial condition ensemble of abrupt4×CO_2 simulations—in which CO_2 is quadrupled at the start and then held constant—with the coupled atmosphere–land–ocean–sea ice Community Earth System Model (CESM1.0.4 with a resolution of roughly 2° in the atmosphere and land and 1° in the ocean and sea ice component; Gent et al. 2011; Danabasoglu et al. 2012). Abrupt forcing allows us to study different time scales, and the conclusions also apply for more realistic gradual forcing scenario simulations, which can be thought of as a convolution of infinitesimal abrupt forcing changes (Good et al. 2011, 2013; Geoffroy et al. 2013a). From a several-century-long control run, each January an ensemble member is branched off. In total, 121 different combinations of ocean, sea ice, and atmospheric states are used as initial conditions for the abrupt CO_2 forcing. This nearly eliminates internal variability when considering the ensemble average. Simulations starting in months other than January were conducted, but yield similar results. All ensemble members are run for 2 years, 13 members

for 100 years, 6 members for 250 years, and one member is run for 1300 years. All atmospheric data shown here are annual anomalies of each ensemble member with respect to the stable annual averaged control run. All oceanic anomalies are the difference of the forced ensemble member and the corresponding years following the control run branch off years, which are up to 100 years apart, to account for the small drift in the control run deep ocean. Ensemble averages are shown, except where noted. Results for other CMIP5 models with a similar experimental setup, but only a few ensemble members are shown by Andrews et al. (2012), Kravitz et al. (2013), Vial et al. (2013), Flato et al. (2014), and Chung and Soden (2015a).

To obtain the forcing, an atmosphere-only control simulation with climatological fixed prescribed SST derived from the coupled control run was run for several decades. Four 30-yr-long quadrupling CO_2 simulations are branched off from different initial conditions. The last 10 years of each simulations' averaged TOA imbalance are depicted as a red cross in Fig. 1. Further, for illustration purpose only, we conduct two more 150-yr step function simulations with $2\times$ and $8\times CO_2$.

3. Forcing adjustment versus time-dependent feedbacks

Figure 1 shows the time evolution of the TOA radiative imbalance, N, against the surface temperature anomaly for all ensemble members of the $4\times CO_2$ step forcing simulations. While little gray dots are annual averages of individual ensemble members, the thick black dots are annual and ensemble means. Starting in the upper left with a temperature increase of 1.1 K in the first year, the climate system evolves toward the equilibrium in the lower right. The linear regression of N against T for the first 150 years (treating the years as independent; black line) leads to the definition of effective radiative forcing (ERF; N at $T = 0$) and effective climate sensitivity (T_{eff}, intersect of regression line with the horizontal axis; e.g., Boucher et al. 2014). The value of T_{eff} is substantially smaller than the equilibrium climate sensitivity (ECS), defined as the intersect of points with horizontal axis ($N_{t\to\infty} = 0$; e.g., Senior and Mitchell 2000; Gregory et al. 2004; Williams et al. 2008; Li et al. 2013; Andrews et al. 2015). Originally, ECS and ERF are defined for doubling of CO_2 concentration from preindustrial values. Throughout this paper we show values for the quadrupling simulations, which can be divided by two to get approximately the standard values for ECS, ERF, and T_{eff}. Deviations from the linear regression imply that a global average λ in Eq. (1) is not constant. This seems to be the case not only on the century time scales, but also over very short time scales of the first few years. To analyze the time evolution of N versus T we discuss two ways to adapt Eq. (1), in both cases by making a first-order perturbation for simplicity. The feedback term could be described as temperature dependent (Armour et al. 2013; Andrews et al. 2015; Gregory et al. 2015):

$$C\frac{dT}{dt} = N = F - \lambda T[1 - f_A(T)]. \tag{2a}$$

Instead, one could treat the climate feedback parameter as constant and adjust the forcing F for processes with a time scale longer than a year, analogously to the tropospheric adjustment due to processes on shorter time scales:

$$C\frac{dT}{dt} = N = F[1 - f_B(t)] - \lambda T. \tag{2b}$$

Note that $f_A(T)$ and $f_B(t)$ are unknown functions. However, by comparing Eqs. (2a) and (2b) for different forcing levels, we can assess which formulation describes the CESM output better. Assume that different step forcing levels F_1, F_2, F_3 (e.g., $2\times CO_2$, $4\times CO_2$, $8\times CO_2$) do relate $F_1 = nF_2 = mF_3$.

We solve Eqs. (2a) and (2b) for T with $C = 7.3\,\mathrm{W\,yr\,m^{-2}\,K^{-1}}$ (Geoffroy et al. 2013a), $\lambda = 1.2\,\mathrm{W\,m^{-2}\,K^{-1}}$ for all cases, and $F = 3.2$, 6.9, and $11.2\,\mathrm{W\,m^{-2}}$ for the different forcing levels. The estimates are based on the years 20 to 100 regression of the CESM $2\times CO_2$, $4\times CO_2$, and $8\times CO_2$ simulations. Note that F is not proportional to the log CO_2 (Gregory et al. 2015, and references therein). For illustrative purposes, we choose $f_A(T)$ as $3.5 - \sqrt{T}0.8$, to make dN/dT decrease as T increases and $f_B(t)$ as exponential functions decaying from $1.3F$ to $0.8F$, to relax dN/dT to a long-term constant value. Figure 2 shows the solution for case A in the leftmost column, case B in the middle, and data from the coupled CESM simulation in the rightmost column. The different forcing levels are depicted in gray, red, and blue.

Because Eq. (2a) is not linear in T, for case A, $T_1(t)$ is different from $nT_2(t)$ or $mT_3(t)$ with the subscripts denoting the use of F_1, F_2, and F_3 (Fig. 2a). The same holds for the TOA radiation imbalance, $N_1(t) \neq nN_2(t) \neq mN_3(t)$ (Fig. 2d). Equation (2b) is linear in T, however, so for case B, $T_1(t) = nT_2(t) = mT_3(t)$ (Fig. 2b), and equivalently for $N(t)$ (Fig. 2e). For CESM, the scaled T (Fig. 2c) and N (Fig. 2f) nearly coincide for the three forcing levels. This indicates that case B and Eq. (2b) constitute a good description of the time evolution of N and T.

The evolution of dN/dT behaves similarly: For case A and Eq. (2a), $dN/dT = -\lambda\{1 - f_A(T) - T[df_A(T)/dT]\}$. The right-hand side depends only on the temperature T

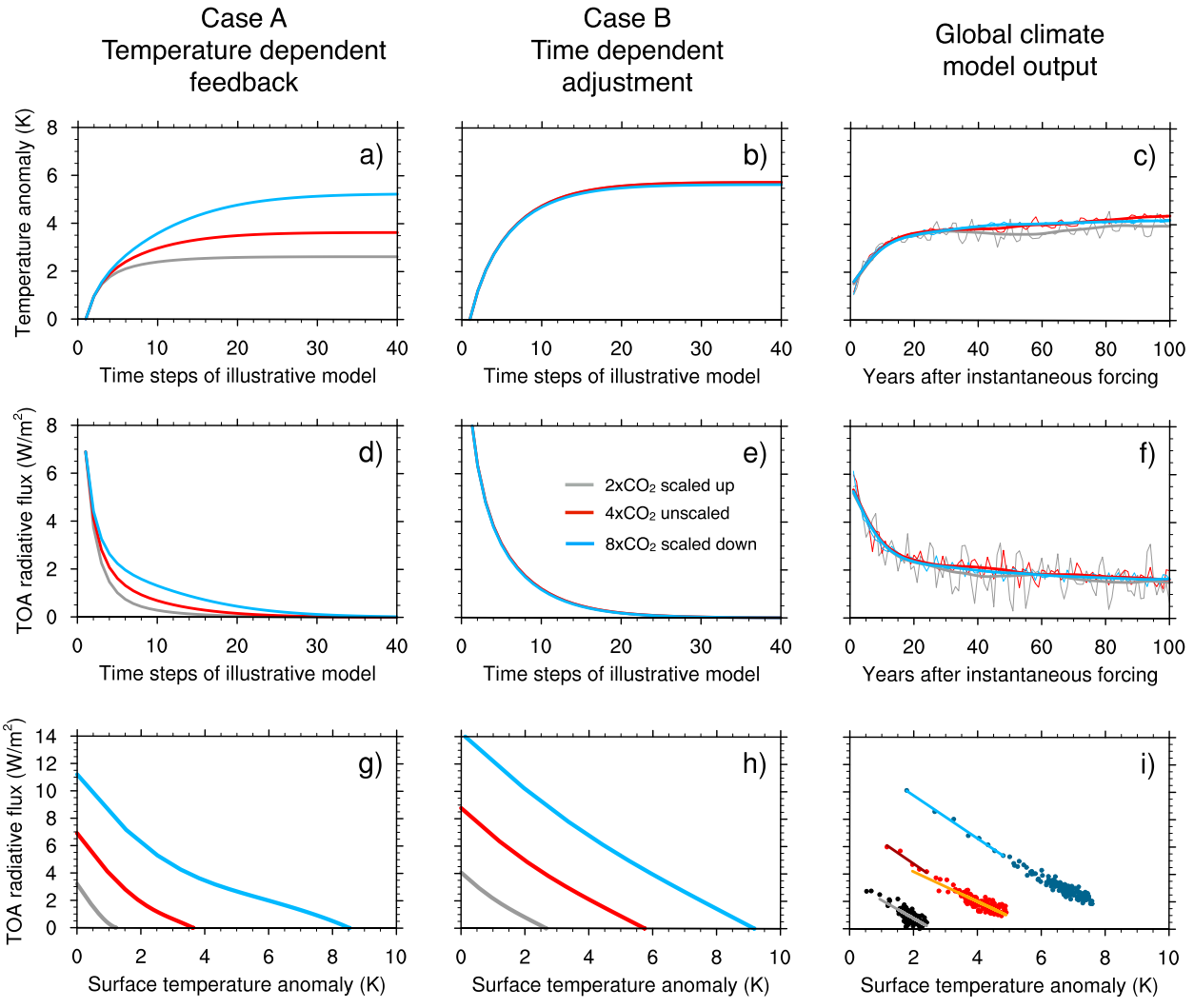

FIG. 2. Illustration of cases A and B, discussed in the text. Scaled temperature anomaly for the illustrative model for (a) case A, (b) case B, and (c) CESM; annual averages are shown by the thin line, and spline fit by the thick line. (d)–(f) As in (a)–(c), but for scaled TOA radiative imbalance. (g)–(i) As in (a)–(c), but for unscaled dT/dN. Gray, red, and light blue depict $2\times CO_2$, $4\times CO_2$, and $8\times CO_2$ forcings, respectively; annual CESM output in (i) is shown in darker colors. The regressions lines (in gray, red, orange, and blue) for different temperature ranges are discussed in the text.

itself and the function $f_A(T)$, assuming λ is constant. This implies that for any given temperature the curves for the different forcing levels have equal dN/dT and are therefore parallel (Fig. 2g, unscaled). For case B, it follows from Eq. (2b) that, at any given time, $dN_1/dT_1 = dN_2/dT_2 = dN_3/dT_3$ (not shown) and any given temperature $dN_1/dT_1 = n(dN_2/dT_2) = m(dN_3/dT_3)$, (Fig. 2h, unscaled). Given the good description of case B and CESM data of N and T over time described above, the fit of dN/dT must be the same (Fig. 2i) CESM data, unscaled). Nevertheless, we test the assumption of case A in Fig. 2i: For two different temperature ranges—in which the data overlap—the slope is indicated. The first range is 0.8–2.5 K, in which $dN_1/dT_1 = 1.32$ (gray) and $dN_2/dT_2 = 1.59$ (dark red). The second range is 1.6–5 K, in which $dN_2/dT_2 = 1.08$ (orange) and $dN_3/dT_3 = 1.56$ (light blue, all in $\mathrm{W\,m^{-2}\,K^{-1}}$). This means the curves are not parallel in the same temperature range (as in Fig. 2g) and case A is not a good description for the CESM data.

In summary, we argue that the curvature in the N–T space for the first few years could be treated as an adjustment problem (case B) rather than a temperature-dependent feedback (case A). This does not imply that later on during the equilibration process the feedback parameter has to be constant, that a combination of cases A and B might not be a better overall description, or that a spatially dependent feedback parameter might be a helpful description (Armour et al. 2013). We now show that the widely used two-box model with an ocean heat

uptake efficacy factor conforms to case B, but modifies the forcing on different time scales than $f_B(t)$.

A commonly used refinement of the global model of Eqs. (2a) and (2b) is to consider two layers (Gregory 2000; Held et al. 2010; Geoffroy et al. 2013a), with T being the temperature of the upper layer and $T_{\text{deep layer}}$ that of the deep layer, and a downward heat flux $\gamma(T - T_{\text{deep layer}})$ between them, with γ being a constant coefficient. Thus, $N = F - \lambda T - \gamma(T - T_{\text{deep layer}})$. To model the apparent nonconstant behavior of λ, it has been proposed to introduce an ocean heat uptake efficacy ε (Winton et al. 2010; Held et al. 2010; Geoffroy et al. 2013b), so that $N = F - \lambda T - (\varepsilon - 1)\gamma(T - T_{\text{deep layer}})$. The overall feedback parameter is initially $\lambda + (\varepsilon - 1)\gamma$, but decreases to λ with the time scale of deep ocean equilibration. Thus, the feedback parameter seems time or state dependent (our case A). There is no detailed physical motivation behind this ansatz, but the suggested mechanism is the poleward shift of ocean heat uptake, which modulates the atmospheric feedbacks. However, this model is linear in T and thus conforms to our case B: $N = F(t)^{\star} - \lambda^{\star} T$, with $F(t)^{\star} = F + (\varepsilon - 1)\gamma T(t)_{\text{deep layer}}$ and $\lambda^{\star} = \lambda + (\varepsilon - 1)\gamma$, which is constant in time, as long as ε and γ do not change through time. Thus, the scaling argument laid out for case B also describes the two-layer model with ocean heat uptake efficacy.

The time scales on which the curvature develops are different in the two models: decades to centuries for $F(T(t)_{\text{deep layer}})$. * and a few years for $f_B(t)$ of our case B. The two models are physically distinct, although formally similar. We do not analyze multidecadal time scales here, which motivated the introduction of ocean heat uptake efficacy. The fast time scale of the two-box model is roughly the same as the time scale of $f_B(t)$ (3–4 yr; Geoffroy et al. 2013b). In the following, we analyze processes setting this time scale in the large ensemble of CESM. These processes may be related to those which set the fast time scale of the two-box model.

In the next section we show how the shortwave cloud radiative response causes the curvature of dN/dT and how the oceanic adjustments—of meridional heat transport, surface heat fluxes, and SST patterns—might be connected to it. Section 5 will come back to the questions whether an adaptation of Eq. (1) according to case B might be useful.

4. From tropospheric to oceanic adjustment

a. Shortwave cloud radiative response

Most studies point to the shortwave cloud response dominating the tropospheric adjustment and the short-term nonlinearity of feedbacks, mostly focusing on the tropical west Pacific (Bala et al. 2010; Colman and McAvaney 2011; Andrews et al. 2012; Zelinka et al. 2013), but also on the Southern Ocean (Grise and Polvani 2014b). We use the measure of cloud radiative effect (CRE) as a rough indication of the cloud response. The CRE is defined as net TOA all-sky minus net clear-sky response and we consider only the shortwave (SW) component, since the longwave component evolves linearly with temperature and shows cloud masking effects. Its applicability is discussed, for example, by Zelinka et al. (2013) and Kamae et al. (2015). On time scales discussed here the SW CRE is dominated by the low-latitude response so that potential aliasing errors over sea ice would be too small to qualitatively impact our results. Figure 3 shows that in agreement with some other studies the SW CRE over the oceans is positive in the first year, and by extrapolation that it is nonzero at $T = 0$, indicating tropospheric adjustment (Colman and McAvaney 2011; Zelinka et al. 2013; Andrews et al. 2015). The SW CRE over the oceans declines as the temperature increases, changes sign after 3 to 4 years, and equilibrates after about a decade at a negative value. Models disagree on the temporal evolution and temperature sensitivity of the SW CRE but many models show a different sensitivity during the first decade compared to the century time scale response (Ringer et al. 2014; also, see gray dots for the global SW CRE response in Fig. 3 herein). In our case, oceanic SW CRE it is not linearly dependent on global mean temperature, as one would expect of a climate feedback. Global SW CRE varies first strongly and on decadal to centennial time scales only very slightly with global mean temperature. This behavior could be described either as an inconstant climate feedback parameter (case A above) or as an adjustment on a longer time scale than a few months (case B). SW CRE over land is also positive in the first year and remains roughly constant, so it can be described as a tropospheric adjustment, with no climate feedback. We will argue below that the SW CRE response comes about not only due to the rapid adjustment to the radiation on monthly time scale, but also due to the oceanic adjustment of heat transport within the first few years after the forcing is applied. We cannot exclude that the surface temperature increase of more than 3 K during the first 10 years influences the SW CRE response. However, Fig. 3 suggests that the SW CRE is not sensitive to temperature anomalies beyond 4 K. The four-member fixed-SST ensemble average SW CRE values (in green and orange for the ocean and land, respectively) lie within the range of the coupled ensembles (i.e., at 0.8 and 0.4 $\mathrm{W\,m^{-2}}$, respectively) with a global surface temperature increase of 0.7 instead of 1.1 K. The standard deviation of the first year's ocean SW CRE is 0.24 $\mathrm{W\,m^{-2}}$, which dominates

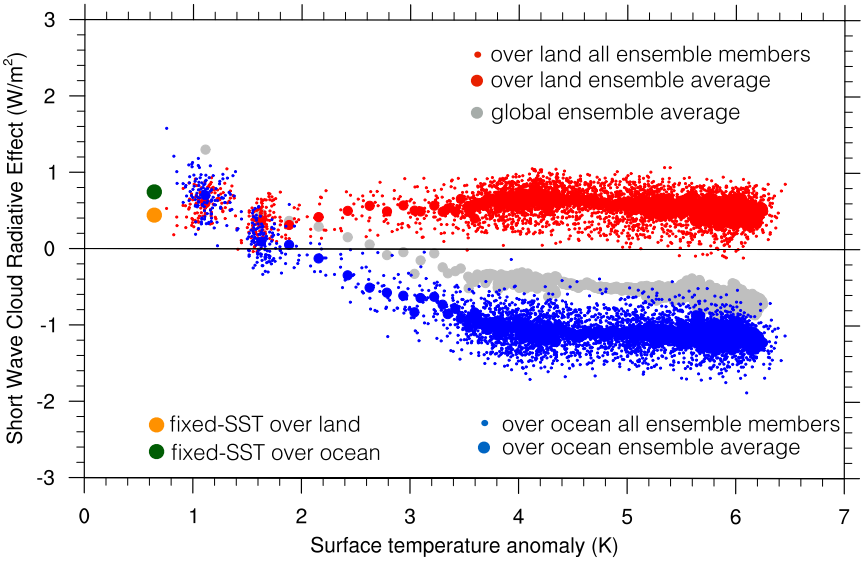

FIG. 3. TOA shortwave cloud radiative effect (positive downward) over land (red), oceans (blue), and total (gray) for all 121 ensemble members of the abrupt4×CO_2 simulations. Small dots depict individual ensemble annual averages, while large dots are ensemble averages (annual until year 100, at ~4.4-K temperature increase, and decadal afterward).

the total TOA ensemble standard deviation of 0.34 W m^{-2} (Fig. 1). The spatial SW CRE response pattern is discussed in section 4d.

b. *Surface temperature, surface heat flux, and ocean heat content patterns*

Figure 4 shows the anomaly patterns of the surface air temperature (leftmost column), sea surface temperature (middle left), surface heat flux (middle right, positive downward), and the rate of change of ocean heat content overlaid by the wind stress (rightmost column) of the first four years (upper four rows) and the long-term average (bottom row). Local values (in K or global W m^{-2}) are divided by their annual global mean value (lower left box in each panel). The surface air and sea temperature increase includes Arctic amplification, enhanced warming over the Northern Hemispheric continents, and initial cooling in the equatorial Pacific region, especially in the east, which gradually weakens. This La Niña–like cooling pattern is attributed to the increase in upwelled cold waters by anomalous surface wind stress forcing (rightmost column). The deep water was not exposed to the surface warming signal yet and increases the east–west temperature gradient across the Pacific (Clement et al. 1996; Cai et al. 2015). The CMIP5 average shows delayed warming in the east Pacific as well (Andrews et al. 2015). Andrews et al. (2015) showed that the evolving pattern of surface warming is the dominant cause of nonlinearity between N and T in Eq. (1) for the HadCM3 and HadGEM2 atmospheric components and that the pattern of SST changes determines the SW CRE.

Taking this line of thought one step further we show in the remainder of this paper how not only SSTs but also the ocean's heat content and transport respond on short time scales and impact the tropospheric response. The two right columns of Fig. 4 show the annual and ensemble average surface heat flux anomaly and the vertically integrated rate of change of ocean heat content. The difference between the two columns is the ocean heat transport convergence. The tropical Atlantic loses heat to the atmosphere (blue in Figs. 4k–n) and the subtropical oceans (blue in Figs. 4p–s) and so does the whole eastern and tropical Pacific. Locally, the time evolution of surface fluxes, heat transport, and surface wind stress are rapidly changing (e.g., in the Indian Ocean, equatorial west Pacific, North Atlantic, or over Eurasia). All responses shown in Fig. 4 in the first four rows are as high as or higher than the inter annual standard deviation of the control run, indicating that they are a forced response. Patterns of surface air and water temperatures in the first years differ strongly from the long-term pattern (Figs. 4e,j). The increase in surface heat flux patchiness (Figs. 4k–o) is dominated by the latent heat flux (not shown). After three years the land does not take up heat. The rate of change of ocean heat content anomaly in year 80–100 (Fig. 4t) is very small and multiplied here by 4 to show the distinctively different pattern in all ocean basins, compared with the initial response pattern. Pattern of heat fluxes from the

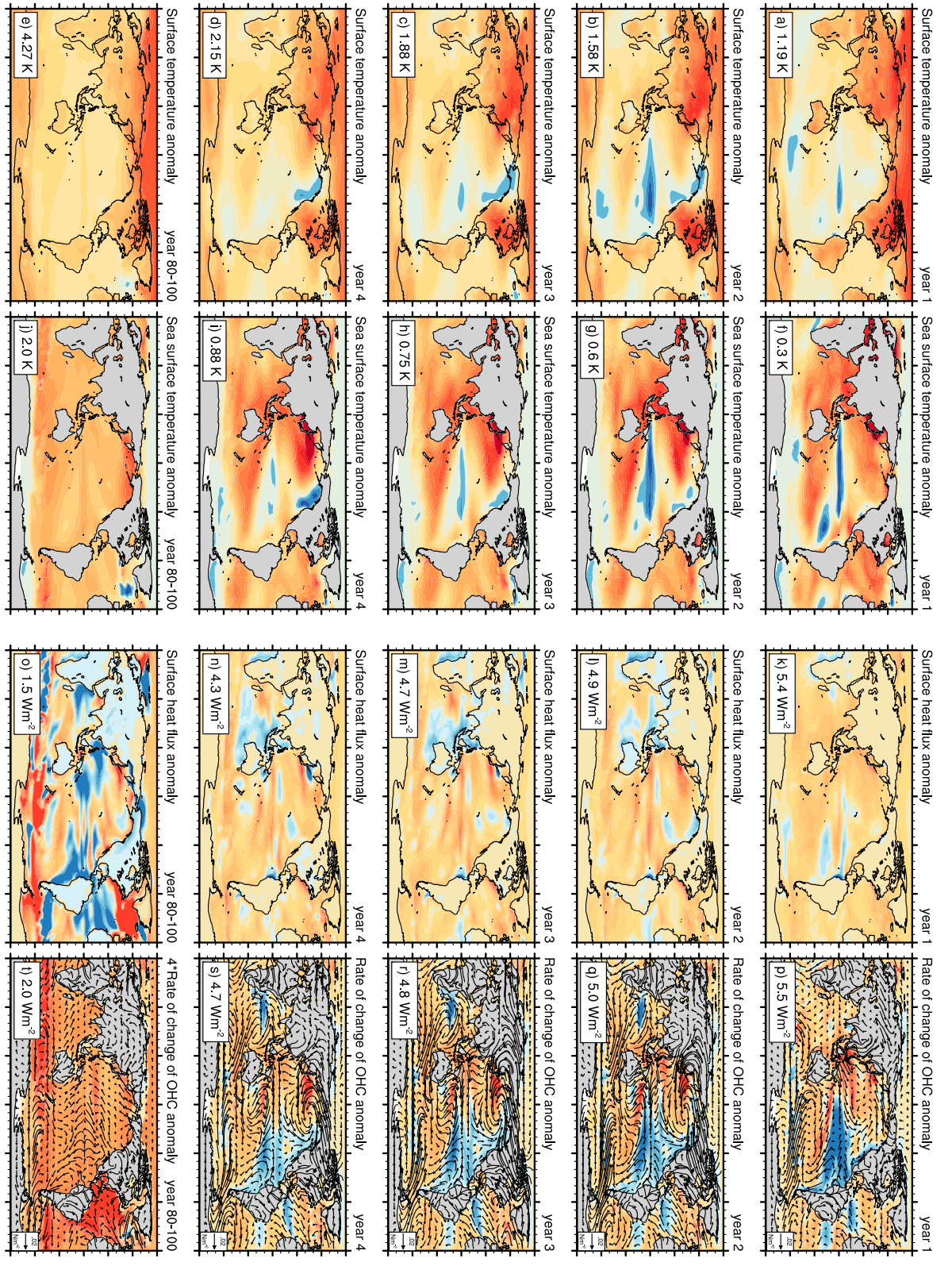

FIG. 4. Abrupt4×CO_2 ensemble and annual mean year one to four and 80–100 for (a)–(e) surface air and (f)–(j) sea temperature anomalies divided by the global response of that year (lower left corner of each panel, in K). Also shown are (k)–(o) surface heat flux anomaly (positive downward) and (p)–(t) rate of change of ocean heat content integrated over the whole water column, again divided by the global value (both W m^{-2}). The difference between the rightmost two columns is the ocean heat transport convergence. Surface wind stress anomaly vectors overlay heat content anomaly contours in the last column.

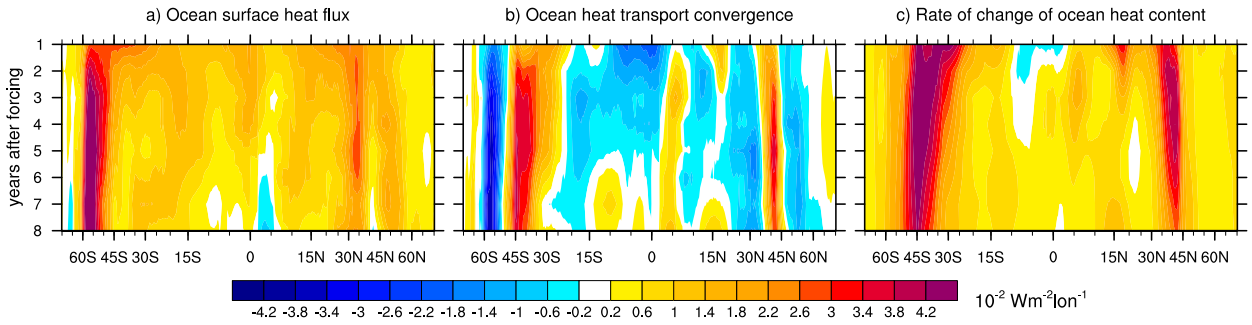

FIG. 5. Abrupt4×CO_2 zonally integrated ensemble and annual mean (a) ocean surface heat flux change, (b) ocean meridional heat transport convergence, and (c) rate of change of ocean heat content, all in Watts per global square meter. Positive values indicate ocean heat uptake in (a), heat accumulation through transport in (b), and an increase in ocean heat content in (c).

mixed layer to the deep ocean can influence atmospheric feedbacks and the global surface temperature response through SW CRE in slab ocean aquaplanet models (Rose et al. 2014). We argue in the following that meridional ocean heat transport shapes SW CRE on short time scales, on which the mixed layer is still equilibrating. A direct comparison to Rose et al. (2014) is not possible given our transient coupled experimental setup. However, their argument that the SST pattern caused by oceanic heat transport influences the SW CRE is the same as laid out here.

We now describe in more detail the oceanic adjustment processes. They are caused by the tropospheric adjustment of the first few months, as well as the anomalous surface heat fluxes, wind stress pattern, and the land–sea warming contrast of the first few years. Since they respond to the forcing and differ from the surface temperature mitigated ocean patterns of decadal to centennial time scales, oceanic adjustments last longer than tropospheric adjustments but provide the lower boundary conditions for the short-term atmospheric response.

c. *Ocean heat transport and circulation response*

Figure 5 shows—as a function of latitude and time—the ensemble mean surface heat flux (Fig. 5a), the meridional ocean heat transport convergence (Fig. 5b), and the rate of change of ocean heat content (Fig. 5c; all in Watts per global square meter). As already obvious from Fig. 4, the zonally integrated anomalous surface heat flux is positive at all latitudes for some years and especially high in the Southern Ocean 50°–60°S and the northern subtropics around 30°N (Fig. 5a). There is anomalous divergence of heat out of the equatorial regions and across the Antarctic circumpolar current (blue in Fig. 5b). These two effects lead to a cooling in the equatorial ocean initially, and warming everywhere else, especially in the midlatitudes, where there is downward wind-driven pumping of heat. The meridional heat transport could be one reason why in the Pacific sea surface temperatures emerge faster than expected from scaling global mean warming (Chadwick et al. 2014). Locally, it can take 2 to 4 years until the fluxes reach their highest value (e.g., around 55°S or 40°N).

In the North Atlantic the short time scale response in surface fluxes leads to a temporary increasing AMOC strength for 2 to 4 years (Fig. 6a), which is statistically different from the year following the branching off in the control run. Based on our simulations we cannot distinguish whether surface freshwater, surface or lateral freshwater fluxes, the wind field anomalies, sea ice edge, or places of convection and deep water formation cause this AMOC response (e.g., Gregory et al. 2005; Smith et al. 2014). All these fields show anomalous patterns in strength and locality compared with the long-term response. The zonally averaged rate of change of ocean heat content the North Atlantic is much smaller than in other locations during the first years and heat reaches depth later (Fig. 7, left minus right column). The wind field anomalies change sign within the first two years (Fig. 4). The small but robust AMOC response shows that even the deep ocean content can be affected by an anomalous surface forcing within a year and local surface conditions can influence volume fluxes elsewhere (e.g., here at 18°S where the overturning response is reversed and delayed for a few years, Fig. 6b). Local surface fluxes and ocean heat uptake efficiency influence the lower boundary condition for the atmosphere to respond to the radiative forcing (Fig. 4) and thus the time scale of tropospheric adjustment and short time scale feedbacks. We trust this surprising result only because of our large ensemble size, with which we can differentiate the response from the control run variability.

Changes in the ocean interior temperature result from the changes in ocean heat transport. Figure 7 shows the global (left) and Pacific (right) ocean heat content change in joules—including surface heat flux and transport—for

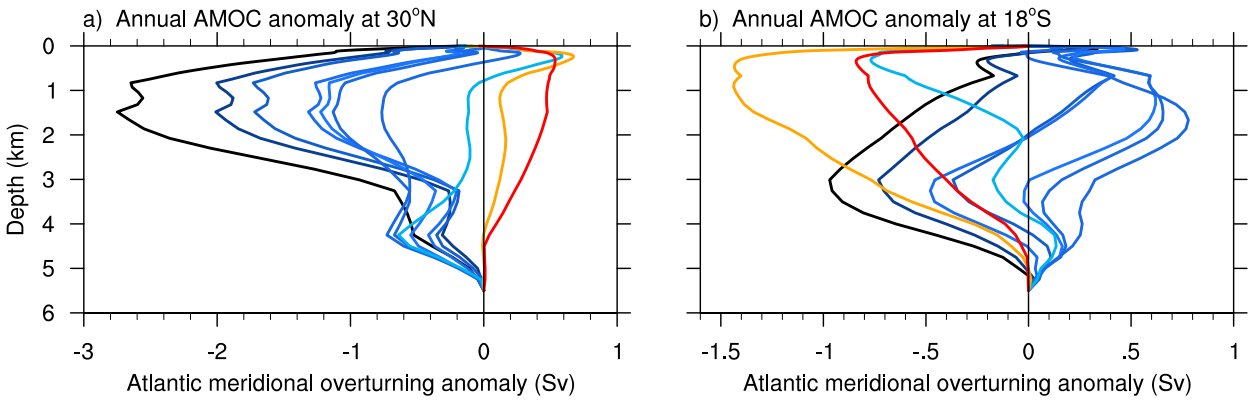

FIG. 6. Abrupt4×CO_2 ensemble and annual mean meridional overturning circulation anomaly at (a) 30°N and (b) 18°S for year 1 (red), year 2 (orange), year 3 (light blue), etc., to year 10 (black) (1 Sv = 10^6 m^3 s^{-1}).

the first four years and the long-term response (lowest row, scaled to compare the patterns and fit the scale). Stippling indicates where the anomalous heat uptake patterns differ from the control run simulation variability at the 95% level. Next to the Pacific subsurface cooling, the nonuniform heating becomes obvious here also with depth. For each location the temperature perturbation reaches depths of 1 km after the first year and in the Southern Ocean the perturbation reaches a depth of 4 km in the second year.

d. Evolution of spatial SW CRE patterns

After having sketched out some processes involved in oceanic adjustment, we now show how the SW CRE responds to the oceanic adjustment. We suggest an interpretation along the lines of case B of section 3.

Figure 8 shows the coupled ensemble average of the first and second year's and the long-term response (Figs. 8a,b,d), and the difference of the fixed-SST response to the first year of the coupled response (Fig. 8c). The fixed-SST response is averaged over years 10 to 30 of four ensemble members and can be regarded as "year 0." In the global mean, the fixed-SST and coupled values are nearly the same [cf. also Fig. 3 herein and the discussion in Ringer et al. (2014)]. However, the spatial pattern shows local differences in the order of magnitude of the response itself, also over the land and especially strongly over the Southern Ocean. Throughout the ensemble, locally the strongest response in magnitude (both positive and negative) appears in year 2 (Fig. 8b). Figure 8d indicates that the long-term response pattern is very different from the short-term response, both in high and low latitudes.

To measure the time evolution of the spatial pattern, and thus the potential to influence the nonlinearity of the feedback term, Fig. 9a shows the root-mean-square difference between each year of each coupled ensemble member and the long-term pattern shown in Fig. 8d. Each ensemble member is depicted as a gray line, and the longer ensemble members as colored lines, for the first 20 years of the simulations. The SW CRE pattern differs strongest from the long-term pattern in year 2 in 74% of all simulations. It takes 5 to 10 years to reduce the deviation from the long-term pattern by half. Figure 9b show that the spread between ensemble members for the first year is dominated by the western equatorial Pacific and Indian Ocean, where the ocean heat transport convergence is also very high and the SST influence the low stratocumulus clouds and thus the SW CRE.

Figures 9c and 9d show again the root-mean-square difference to the long-term pattern of the rate of ocean heat content change and SSTs, which are similar to the response of SW CRE. To remove the global warming signal, the SST and dOHC/dt patterns are normalized with their global values, as in Fig. 4, before the root-mean-square difference is computed. The SW CRE pattern, however, is not normalized, since it does not scale with global mean temperature anomaly as a feedback would do. The time scale of pattern changes of SW CRE, rate of heat content change, and the SST are similar; most changes happen in the first six years. We interpret this as an indication that the SW CRE response over the ocean—after being triggered by the application of the forcing—is shaped by the oceanic adjustment of heat transport to the forcing. Perturbed physics experiments fixing the clouds or ocean heat transport would be necessary to understand this relationship in more detail. The analysis here shows that even very short time scales should be studied in coupled atmosphere–ocean instead of fixed-SST or slab ocean frameworks.

5. Virtual radiative forcing

We have shown in section 4 why fixed-SST simulations do not represent the full magnitude of the adjustment

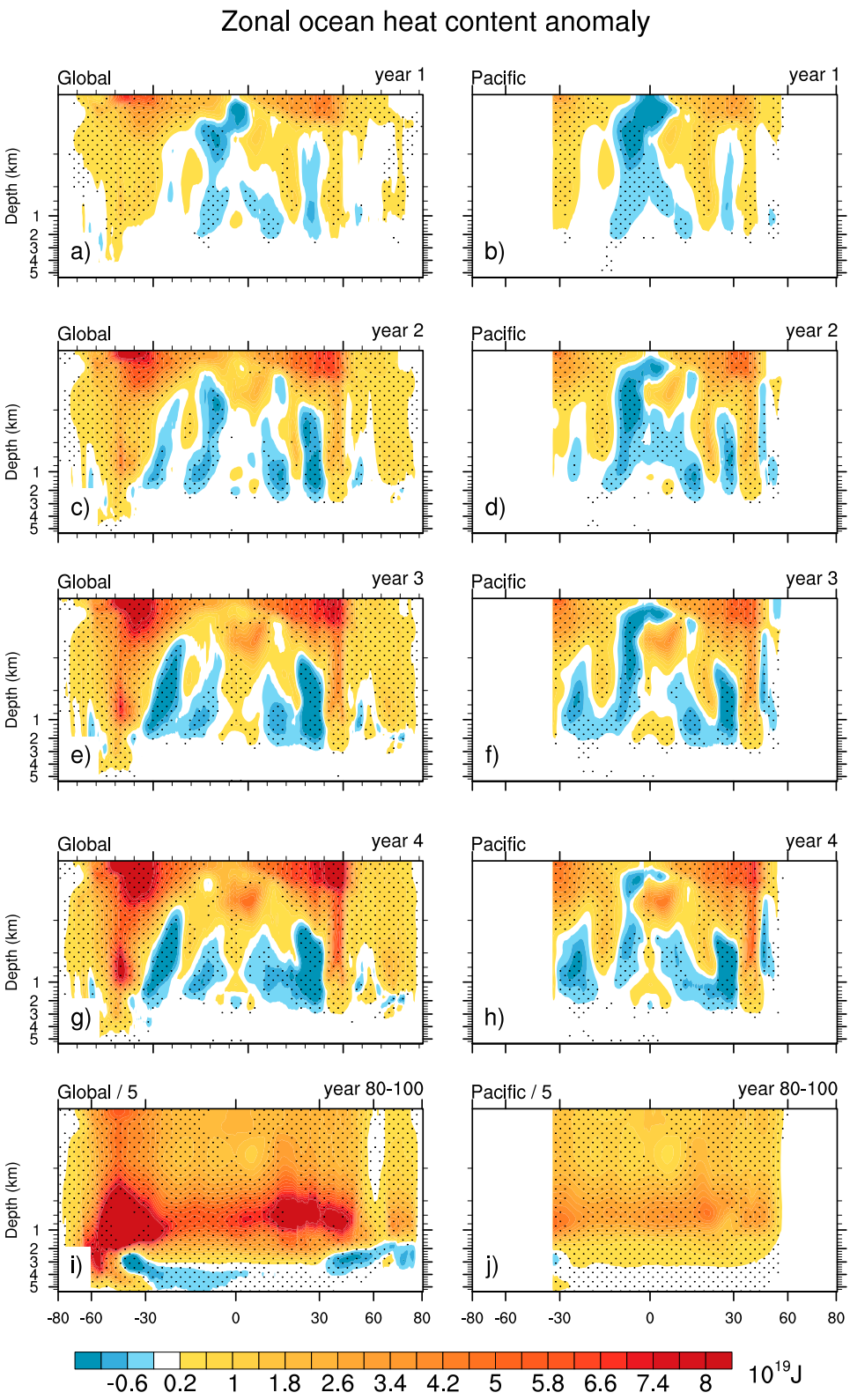

FIG. 7. Abrupt4×CO_2 ensemble mean (left) global and (right) Pacific ocean heat content change for (top 4 rows) the end of years 1 to 4 and (bottom) the average of years 80–100 divided by 5 to fit the scale. Stippling indicates that the anomaly is significantly different from the control run variability at the 95% level.

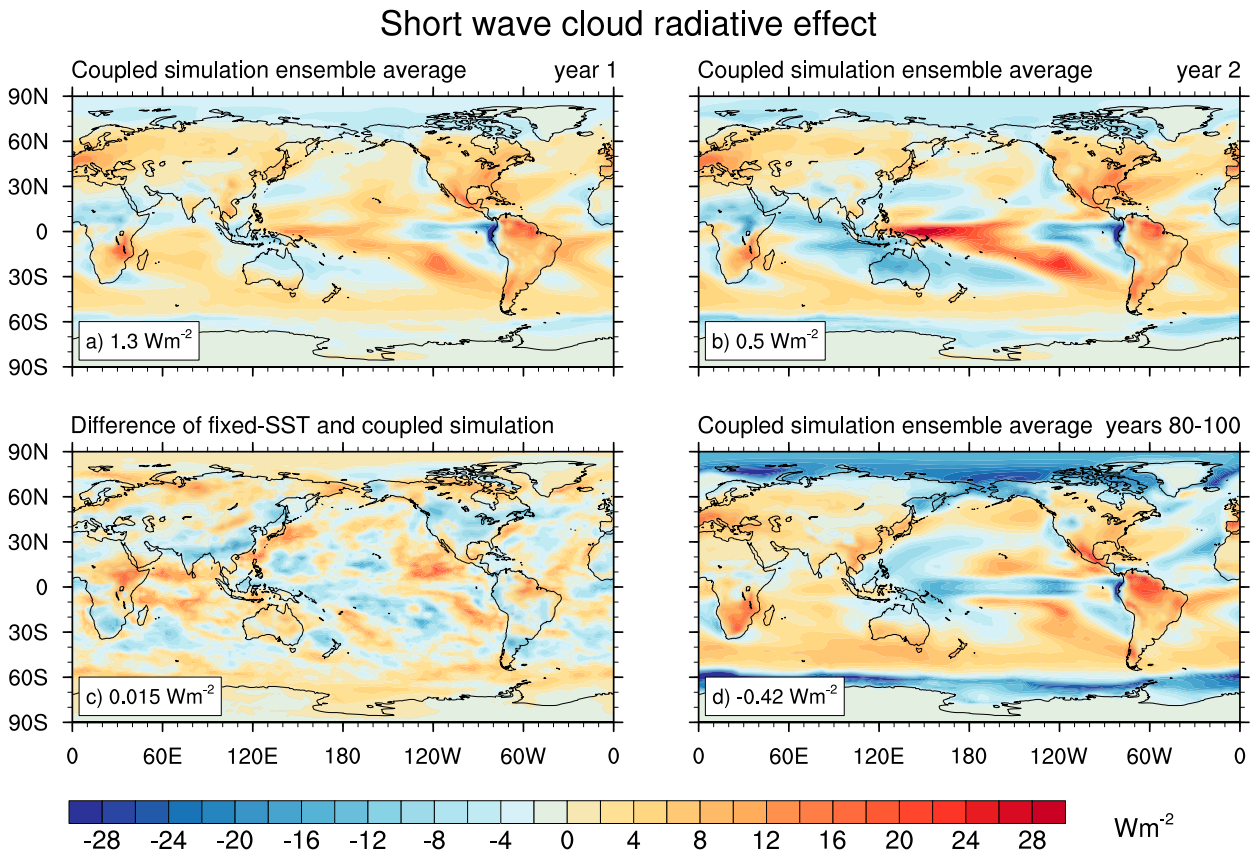

FIG. 8. Abrupt4×CO_2 shortwave cloud radiative effect for the (a) first and (b) second year, and (d) the long-term coupled ensemble average. (c) Difference between the fixed-SST ensemble average of years 10–30 and the average coupled response of the first year. Global values are indicated in the lower left corner of each panel, all in W m^{-2} for the whole global area.

processes and discussed which oceanic processes could play a role in the adjustment process. In section 3 we suggested that the forcing term could be modified to capture the nonlinear evolution of dN/dT. We now propose a formulation of the forcing term, which includes processes of oceanic adjustments and reattributes part of the N–T curvature to the forcing. If fixed-SST simulations do not represent the full tropospheric adjustment magnitude, which forcing do they represent? Figure 1 indicates that the fixed-SST forcing is smaller than the ERF obtained in a regression of the first 150 years. In Flato et al. (2014) 5 out of 10 CMIP5 models, which contributed both the forcing from fixed-SST and the regression method, had smaller or similar forcings obtained by both methods. The brown cross in Figs. 10a and 10b includes the correction suggested by Hansen et al. (2005), using the 150-yr regression (from Fig. 1) to project F_{fixedSST} (red cross) onto the vertical axis. This assumes that the same feedbacks act in a fixed-SST and coupled run and that λ is constant, which is both not the case (e.g., Gregory and Webb 2008). The orange cross adds the land warming of around 0.4 W m^{-2} to the fixed-SST forcing. Finally as an example, the green cross is the intersection of the vertical axis with the regression of years 10–150 (red line). This somewhat arbitrary time frame takes into account all adjustment and ocean mixed layer processes of the first 10 years.

a. *Alternative method to obtain* F *and* λ*: Moving window regression*

To examine the nonconstancy of F and λ in more detail, we now regress the radiative imbalance not over a certain time, but over a limited temperature range. That is equivalent to calculating the local derivative $\Delta N/\Delta T$ and the corresponding axes' intersects for that regression. The blue shaded area in Fig. 10a is the first temperature window, starting at 0.6 K and ranging up to 2 K. The lower bound is set by the first year's temperature of the coldest ensemble member, while the range of 1.4 K is chosen to be large enough to include at least three years. This prevents regressing members of only one year, while keeping the window small enough to resolve the time or temperature dependence of the feedback parameter. The method is similar to the binned regression of Block and

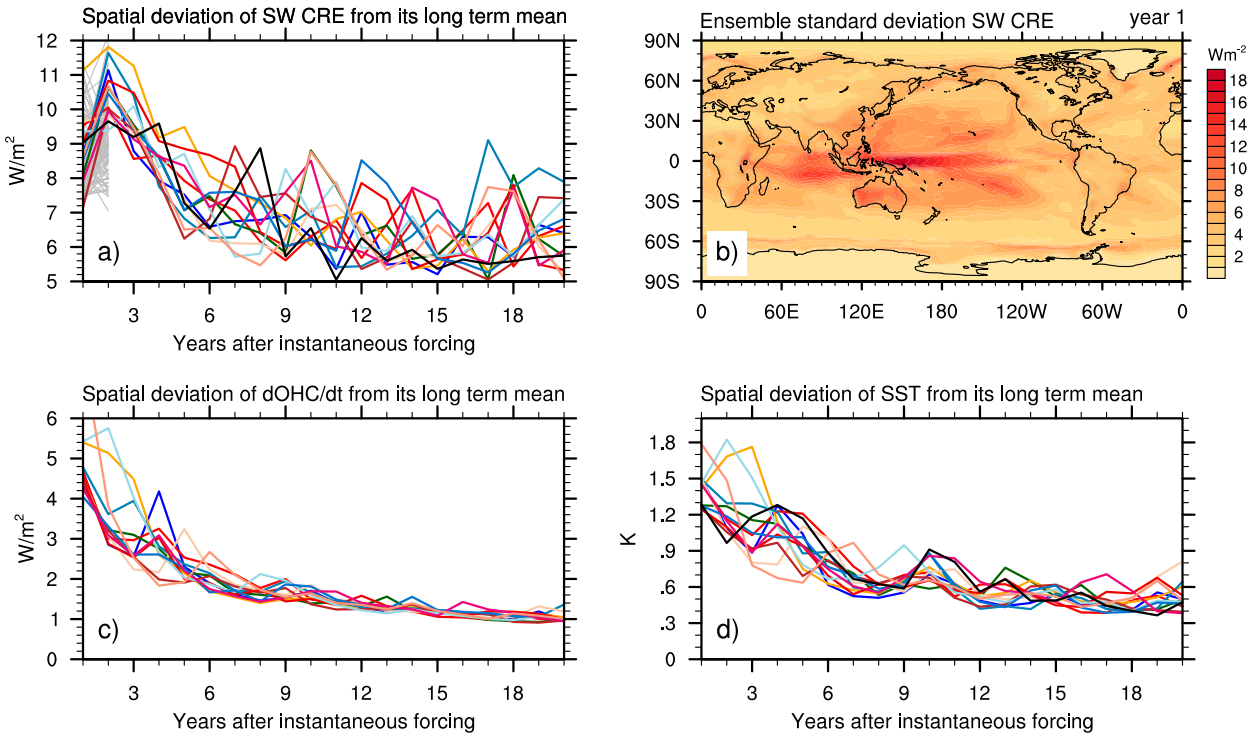

FIG. 9. Abrupt4×CO_2 coupled ensemble member (colors and gray). (a) Root-mean-square deviation of the spatial SW CRE pattern from the long-term ensemble average pattern shown in Fig. 8d. (b) SW CRE standard deviation of coupled ensemble. (c) Root-mean-square deviation of rate of change of ocean heat content from its long-term pattern shown in Fig. 4t. (d) Root-mean-square deviation of rate of SST from its long-term pattern shown in Fig. 4j. Patterns used for (c) and d) are normalized, as in Fig. 4.

Mauritsen (2013), Ringer et al. (2014), or Andrews et al. (2015), who regress N against T for a certain range of time. While these studies use only time frames (e.g., years 1–20 vs 20–150), we move the window continuously through the whole temperature range of the first 30 years in 0.1 K steps (gray in Fig. 10a), while recording the slope and axis intersects (blue regression line for the first window in blue shading). A centennial perspective of this method is presented by Knutti and Rugenstein (2015). An advantage of the large ensemble is that each bin has more similar numbers of points, so the comparison between regression attributes is more robust than

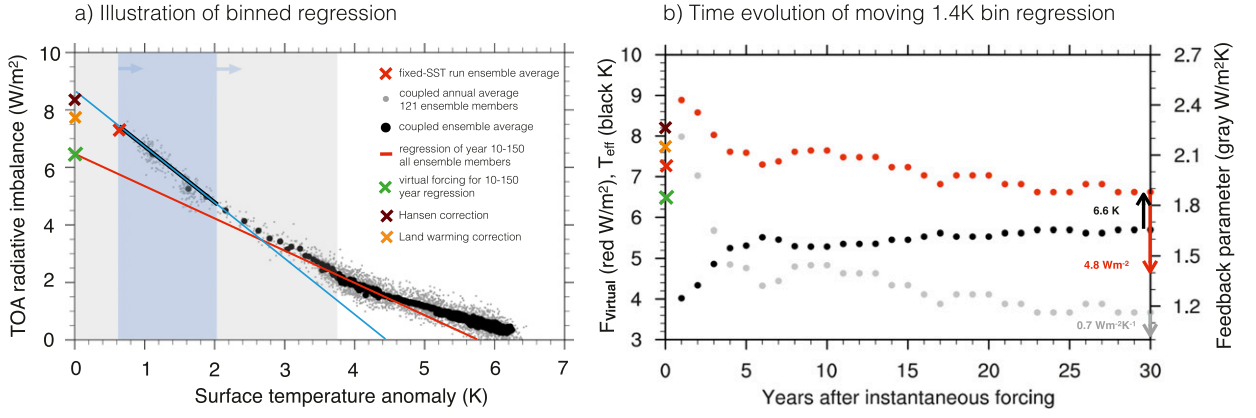

FIG. 10. (a) Annual global mean TOA net downward radiative flux evolution against global average surface air temperature anomaly, regressed for years 10 to 150 (red), and example of 1.4-K wide window to determine the time dependence of T_{eff}, F_{virtual}, and λ (blue). (b) Time evolution of T_{eff} (black), F_{virtual} (red), and λ (gray) for the time and temperature range indicated by the gray shading in (a). Values and arrows at the right vertical axis are the values of the same method after 150 yr.

comparing, for example, a regression of 10 versus 140 points. All values are then transferred from the temperature back to the time domain (horizontal axis in Fig. 10b). The overall shape of the time dependence in Fig. 10b is not sensitive to the regression bin width or the use of annual or decadal averaged data. Figure 10b shows that the first five to six years contribute most to the effect of T_{eff}, ERF, and λ not being constant on short time scales. After 30 years T_{eff} is still more than 0.8 K away from the approximate 6.6 K ECS. The same holds for λ and ERF, indicated by the arrows and 150-yr values on the right axis.

We suggest to call a forcing not obtained by regressing the first 150 years, but any other time frame virtual forcing. Virtual since there is no real state that experiences that forcing (Andrews et al. 2015), and since it is not only a radiative forcing but includes the whole state of the coupled system. Certain processes are fully, others only partly, included: for example, the virtual forcing of year 5 ($7.6\,\mathrm{W\,m^{-2}}$) includes the adjustment of the AMOC and the corresponding influence on ocean heat uptake but only (although the main) part of the SW CRE adjustment.

b. Applications and limitations

The virtual forcing could be chosen simply as the forcing value that is most suited to maintain a ''linear enough'' relationship between N and T in a desired range of temperature or time in order to answer a certain question. While this approach complicates the definition of the forcing term, it might shift the attention to understanding and comparing processes step by step. If the initial curvature in dN/dT is indeed explained through a modified forcing term, the use of a virtual forcing would help to differentiate responses caused by the application of the forcing and the surface temperature increase. Ringer et al. (2014) found a correlation between the forcing term and the SW cloud feedback over 150 years. Folding these processes into the forcing term might be helpful to disentangle forcing and feedback. The concept of virtual forcing also might help to compare models with different degrees of adjustment. Assume that one model X has a strong sea ice response within the first three years, while model Y has a strong west Pacific SW CRE response within the first two years, and model Z shows a perfectly linear N–T relationship over the first few years. Comparing their virtual forcings might be cleaner than comparing their ERF or fixed-SST forcings, leading to a reduced uncertainty in λ and ECS. Given the evolution of λ, F, and ECS term in Fig. 10 it is also unclear which forcing is most suitable to determine ECS from observations (e.g., Otto et al. 2013) and how representative the transient response at any time is not only of equilibrium conditions, but also of any other time frame (Gregory et al. 2015). The virtual radiative forcing has the potential to be more process based than the ERF or fixed-SST forcing. Finally, one might use the virtual forcing for more technical studies: Even in noncoupled simulations one might differentiate with this method between specific atmospheric processes (e.g., by keeping the land surface temperature, certain surface fluxes, or aerosol concentrations fixed) and determine their adjustment time scales.

One obvious limitation becomes clear in Fig. 10b and by recalling the formulation of case B: The description of the time dependency of the adjustment might be more complicated than the exponential illustrative example in section 3. Note that $f_B(t)$ does not have an obvious formulation and depends on various very likely strongly model-dependent processes. In the coupled model reality, temperature-dependent processes (either in the form of case A or related to the deep ocean equilibration) can set in while a model is still adjusting. Thus, it is open to which degree the concept described here might be indeed helpful, not only in a model context with clearly defined forcing (here only done for one CO_2 level) and a rough understanding of internal variability, but also concerning observational estimates of surface warming and ocean heat uptake.

6. Conclusions

We use a 121-member ensemble of abrupt4×CO_2 simulations to overcome initial conditions dependency and internal variability to explore the heat flux through the coupled system within the first few years after an abrupt forcing. After the forcing is applied, the stratosphere and troposphere adjust within a few months. The resulting anomalous surface flux and wind stress force the ocean to take up and transport heat meridionally and vertically. Locally, the meridional ocean heat transport convergence can be even stronger than the surface heat flux, leading to a short-term tropical Pacific cooling. Circulation adjustments include the Atlantic meridional overturning circulation, which increases for some years. These oceanic adjustments of circulation and heat transport set the conditions for local surface fluxes and thus the atmospheric response of the first few years. The SW CRE over the oceans in particular has an adjustment time scale of several years, after which it does not scale with the global mean atmospheric temperature increase like a feedback would do. Instead, the time scale of pattern formation of SW CRE, SST, and ocean heat transport convergence from their initial homogeneous to a spatially stable pattern changing only in magnitude is the same. The time scale discussed here is connected to the fast time scales identified by, for

instance, Hasselmann et al. (1993), Held et al. (2010), Caldeira and Myhrvold (2013), or Geoffroy et al. (2013b). Simple energy balance models or fits to coupled model output may capture part of the behavior but might be a less helpful framework to understand processes. We show through scaling an abrupt2×CO_2 and 8×CO_2 simulation that the coupled model output is better described as a forcing adjustment than as a temperature dependent feedback. In other words, the processes causing the curvature of dN/dT during the first few years proceed with a characteristic time scale in response to the forcing [Eq. (2b)] and do not scale nonlinearly with the global mean temperature [Eq. (2a)].

We define a virtual forcing—a variation of the traditional forcing term, which is defined either as effective radiative forcing or fixed-SST forcing. Virtual forcing is the forcing at a time when the feedback parameter is approximately constant in the time range of interest. Folding adjustment processes into the forcing term might help to compare models with different adjustment processes, to circumvent forcing-feedback correlations, or potentially also to better estimate ECS from observed warming and ocean heat uptake (Otto et al. 2013; Knutti and Rugenstein 2015). However, in principle a model could adjust for a few years through various processes and then either remain linear or display nonlinear feedbacks. At this stage it is unclear whether there is a sufficiently robust behavior across models that the concept can be useful. We do not want to argue that this approach is superior to describing the feedbacks as time or state dependent but simply offer one more approach in the recent discussion of the forcing-feedback framework applicability.

Acknowledgments. We thank three anonymous reviewers, Mike Winton, and Bala Govindasamy for their interest and stimulating in-depth comments.

REFERENCES

Andrews, T., and P. M. Forster, 2008: CO_2 forcing induces semi-direct effects with consequences for climate feedback interpretations. *Geophys. Res. Lett.*, **35**, L04802, doi:10.1029/2007GL032273.

——, ——, O. Boucher, N. Bellouin, and A. Jones, 2010: Precipitation, radiative forcing and global temperature change. *Geophys. Res. Lett.*, **37**, L14701, doi:10.1029/2010GL043991.

——, J. M. Gregory, M. J. Webb, and K. E. Taylor, 2012: Forcing, feedbacks and climate sensitivity in CMIP5 coupled atmosphere–ocean climate models. *Geophys. Res. Lett.*, **39**, L09712, doi:10.1029/2012GL051607.

——, ——, and ——, 2015: The dependence of radiative forcing and feedback on evolving patterns of surface temperature change in climate models. *J. Climate*, **28**, 1630–1648, doi:10.1175/JCLI-D-14-00545.1.

Armour, K. C., C. M. Bitz, and G. H. Roe, 2013: Time-varying climate sensitivity from regional feedbacks. *J. Climate*, **26**, 4518–4534, doi:10.1175/JCLI-D-12-00544.1.

Bala, G., K. Caldeira, and R. Nemani, 2010: Fast versus slow response in climate change: Implications for the global hydrological cycle. *Climate Dyn.*, **35**, 423–434, doi:10.1007/s00382-009-0583-y.

Block, K., and T. Mauritsen, 2013: Forcing and feedback in the MPI-ESM-LR coupled model under abruptly quadrupled CO_2. *J. Adv. Model. Earth Syst.*, **5**, 676–691, doi:10.1002/jame.20041.

Bony, S., G. Bellon, D. Klocke, S. Sherwood, S. Fermepin, and S. Denvil, 2013: Robust direct effect of carbon dioxide on tropical circulation and regional precipitation. *Nat. Geosci.*, **6**, 447–451, doi:10.1038/ngeo1799.

Boucher, O., and Coauthors, 2014: Clouds and aerosols. *Climate Change 2013: The Physical Science Basis*, Cambridge University Press, 571–657.

Cai, W., and Coauthors, 2015: Increased frequency of extreme La Niña events under greenhouse warming. *Nat. Climate Change*, **5**, 132–137, doi:10.1038/nclimate2492.

Caldeira, K., and N. P. Myhrvold, 2013: Projections of the pace of warming following an abrupt increase in atmospheric carbon dioxide concentration. *Environ. Res. Lett.*, **8**, 034039, doi:10.1088/1748-9326/8/3/034039.

Cao, L., G. Bala, and K. Caldeira, 2011: Why is there a short-term increase in global precipitation in response to diminished CO_2 forcing? *Geophys. Res. Lett.*, **38**, L06703, doi:10.1029/2011GL046713.

——, ——, and ——, 2012: Climate response to changes in atmospheric carbon dioxide and solar irradiance on the time scale of days to weeks. *Environ. Res. Lett.*, **7**, 034015, doi:10.1088/1748-9326/7/3/034015.

Chadwick, R., P. Good, T. Andrews, and G. Martin, 2014: Surface warming patterns drive tropical rainfall pattern responses to CO_2 forcing on all timescales. *Geophys. Res. Lett.*, **41**, 610–615, doi:10.1002/2013GL058504.

Chung, E.-S., and B. J. Soden, 2015a: An assessment of direct radiative forcing, radiative adjustments, and radiative feedbacks in coupled ocean–atmosphere models. *J. Climate*, **28**, 4152–4170, doi:10.1175/JCLI-D-14-00436.1.

——, and ——, 2015b: An assessment of methods for computing radiative forcing in climate models. *Environ. Res. Lett.*, **10**, 074004, doi:10.1088/1748-9326/10/7/074004.

Clement, A. C., R. Seager, M. A. Cane, and S. E. Zebiak, 1996: An ocean dynamical thermostat. *J. Climate*, **9**, 2190–2196, doi:10.1175/1520-0442(1996)009<2190:AODT>2.0.CO;2.

Colman, R., and B. McAvaney, 2011: On tropospheric adjustment to forcing and climate feedbacks. *Climate Dyn.*, **36**, 1649–1658, doi:10.1007/s00382-011-1067-4.

Danabasoglu, G., S. C. Bates, B. P. Briegleb, S. R. Jayne, M. Jochum, W. G. Large, S. Peacock, and S. G. Yeager, 2012: The CCSM4 ocean component. *J. Climate*, **25**, 1361–1389, doi:10.1175/JCLI-D-11-00091.1.

Dong, B., J. M. Gregory, and R. T. Sutton, 2009: Understanding land–sea warming contrast in response to increasing greenhouse gases. Part I: Transient adjustment. *J. Climate*, **22**, 3079–3097, doi:10.1175/2009JCLI2652.1.

Doutriaux-Boucher, M., M. J. Webb, J. M. Gregory, and O. Boucher, 2009: Carbon dioxide induced stomatal closure increases radiative forcing via a rapid reduction in low cloud. *Geophys. Res. Lett.*, **36**, L02703, doi:10.1029/2008GL036273.

Flato, G., and Coauthors, 2014: Evaluation of climate models. *Climate Change 2013: The Physical Science Basis*, T. F. Stocker et al., Eds., Cambridge University Press, 741–866.

Forster, P. M., T. Andrews, P. Good, J. M. Gregory, L. S. Jackson, and M. Zelinka, 2013: Evaluating adjusted forcing and model spread for historical and future scenarios in the CMIP5 generation of climate models. *J. Geophys. Res. Atmos.*, **118**, 1139–1150, doi:10.1002/jgrd.50174.

Gent, P. R., and Coauthors, 2011: The Community Climate System Model version 4. *J. Climate*, **24**, 4973–4991, doi:10.1175/2011JCLI4083.1.

Geoffroy, O., D. Saint-Martin, D. J. L. Olivié, A. Voldoire, G. Bellon, and S. Tytéca, 2013a: Transient climate response in a two-layer energy-balance model. Part I: Analytical solution and parameter calibration using CMIP5 AOGCM experiments. *J. Climate*, **26**, 1841–1857, doi:10.1175/JCLI-D-12-00195.1.

——, ——, G. Bellon, A. Voldoire, D. J. L. Olivié, and S. Tytéca, 2013b: Transient climate response in a two-layer energy-balance model. Part II: Representation of the efficacy of deep-ocean heat uptake and validation for CMIP5 AOGCMs. *J. Climate*, **26**, 1859–1876, doi:10.1175/JCLI-D-12-00196.1.

Good, P., J. M. Gregory, and J. A. Lowe, 2011: A step-response simple climate model to reconstruct and interpret AOGCM projections. *Geophys. Res. Lett.*, **38**, L01703, doi:10.1029/2010GL045208.

——, ——, ——, and T. Andrews, 2013: Abrupt CO_2 experiments as tools for predicting and understanding CMIP5 representative concentration pathway projections. *Climate Dyn.*, **40**, 1041–1053, doi:10.1007/s00382-012-1410-4.

Gregory, J. M., 2000: Vertical heat transports in the ocean and their effect on time-dependent climate change. *Climate Dyn.*, **16**, 501–515, doi:10.1007/s003820000059.

——, and M. Webb, 2008: Tropospheric adjustment induces a cloud component in CO_2 forcing. *J. Climate*, **21**, 58–71, doi:10.1175/2007JCLI1834.1.

——, and Coauthors, 2004: A new method for diagnosing radiative forcing and climate sensitivity. *Geophys. Res. Lett.*, **31**, L03205, doi:10.1029/2003GL018747.

——, and Coauthors, 2005: A model intercomparison of changes in the Atlantic thermohaline circulation in response to increasing atmospheric CO_2 concentration. *Geophys. Res. Lett.*, **32**, L12703, doi:10.1029/2005GL023209.

——, T. Andrews, and P. Good, 2015: The inconstancy of transient climate sensitivity under increasing CO_2. *Philos. Trans. Roy. Soc. London*, **373A**, 20140417, doi:10.1098/rsta.2014.0417.

Grise, K. M., and L. M. Polvani, 2014a: Southern Hemisphere cloud–dynamics biases in CMIP5 models and their implications for climate projections. *J. Climate*, **27**, 6074–6092, doi:10.1175/JCLI-D-14-00113.1.

——, and ——, 2014b: The response of mid-latitude jets to increased CO_2: Distinguishing the roles of sea surface temperature and direct radiative forcing. *Geophys. Res. Lett.*, **41**, 6863–6871, doi:10.1002/2014GL061638.

Hansen, J., and Coauthors, 2005: Efficacy of climate forcings. *J. Geophys. Res.*, **110**, D18104, doi:10.1029/2005JD005776.

Hasselmann, K., R. Sausen, E. Maier-Reimer, and R. Voss, 1993: On the cold start problem in transient simulations with coupled atmosphere–ocean models. *Climate Dyn.*, **9**, 53–61, doi:10.1007/BF00210008.

Held, I., M. Winton, K. Takahashi, T. L. Delworth, F. Zeng, and G. Vallis, 2010: Probing the fast and slow components of global warming by returning abruptly to preindustrial forcing. *J. Climate*, **23**, 2418–2427, doi:10.1175/2009JCLI3466.1.

Kamae, Y., and M. Watanabe, 2013: Tropospheric adjustment to increasing CO_2: Its timescale and the role of land–sea contrast. *Climate Dyn.*, **41**, 3007–3024, doi:10.1007/s00382-012-1555-1.

——, ——, T. Ogura, M. Yoshimori, and H. Shiogama, 2015: Rapid adjustments of cloud and hydrological cycle to increasing CO_2: A review. *Current Climate Change Rep.*, **1**, 103–113, doi:10.1007/s40641-015-0007-5.

Knutti, R., and M. A. A. Rugenstein, 2015: Feedbacks, climate sensitivity and the limits of linear models. *Philos. Trans. Roy. Soc. London*, **373A**, 20140428, doi:10.1098/rsta.2015.0146.

Kravitz, B., and Coauthors, 2013: An energetic perspective on hydrological cycle changes in the geoengineering model intercomparison project. *J. Geophys. Res. Atmos.*, **118**, 13 087–13 102, doi:10.1002/2013JD020502.

Lahellec, A., and J.-L. Dufresne, 2014: A formal analysis of the feedback concept in climate models. Part II: Tangent linear systems in GCMs. *J. Atmos. Sci.*, **71**, 3350–3375, doi:10.1175/JAS-D-13-0334.1.

Lambert, F. H., and N. E. Faull, 2007: Tropospheric adjustment: The response of two general circulation models to a change in insolation. *Geophys. Res. Lett.*, **34**, L03701, doi:10.1029/2006GL028124.

Larson, E. J. L., and R. W. Portmann, 2015: A temporal kernel method to compute effective radiative forcing in CMIP5 transient simulations. *J. Climate*, **29**, 1497–1509, doi:10.1175/JCLI-D-15-0577.1.

Li, C., J.-S. von Storch, and J. Marotzke, 2013: Deep-ocean heat uptake and equilibrium climate response. *Climate Dyn.*, **40**, 1071–1086, doi:10.1007/s00382-012-1350-z.

Long, M. C., K. Lindsay, S. Peacock, J. K. Moore, and S. C. Doney, 2013: Twentieth-century oceanic carbon uptake and storage in CESM1(BGC). *J. Climate*, **26**, 6775–6800, doi:10.1175/JCLI-D-12-00184.1.

Meraner, K., T. Mauritsen, and A. Voigt, 2013: Robust increase in equilibrium climate sensitivity under global warming. *Geophys. Res. Lett.*, **40**, 5944–5948, doi:10.1002/2013GL058118.

Merlis, T. M., 2015: Direct weakening of tropical circulations from masked CO_2 radiative forcing. *Proc. Natl. Acad. Sci. USA*, **112**, 13 167–13 171, doi:10.1073/pnas.1508268112.

Otto, A., and Coauthors, 2013: Energy budget constraints on climate response. *Nat. Geosci.*, **6**, 415–416, doi:10.1038/ngeo1836.

Ringer, M. A., T. Andrews, and M. J. Webb, 2014: Global-mean radiative feedbacks and forcing in atmosphere-only and coupled atmosphere–ocean climate change experiments. *Geophys. Res. Lett.*, **41**, 4035–4042, doi:10.1002/2014GL060347.

Rogelj, J., and Coauthors, 2011: Emission pathways consistent with a 2°C global temperature limit. *Nat. Climate Change*, **1**, 413–418, doi:10.1038/nclimate1258.

Rose, B. E. J., K. C. Armour, D. S. Battisti, N. Feldl, and D. D. B. Koll, 2014: The dependence of transient climate sensitivity and radiative feedbacks on the spatial pattern of ocean heat uptake. *Geophys. Res. Lett.*, **41**, 1071–1078, doi:10.1002/2013GL058955.

Schaller, N., J. Cermak, M. Wild, and R. Knutti, 2013: The sensitivity of the modeled energy budget and hydrological cycle to CO_2 and solar forcing. *Earth Syst. Dyn.*, **4**, 253–266, doi:10.5194/esd-4-253-2013.

Senior, C. A., and J. F. B. Mitchell, 2000: The time-dependence of climate sensitivity. *Geophys. Res. Lett.*, **27**, 2685–2688, doi:10.1029/2000GL011373.

Sherwood, S. C., S. Bony, O. Boucher, C. Bretherton, P. M. Forster, J. M. Gregory, and B. Stevens, 2014: Adjustments in the forcing-feedback framework for understanding climate change. *Bull. Amer. Meteor. Soc.*, **96**, 217–228, doi:10.1175/BAMS-D-13-00167.1.

Shine, K. P., R. Derwent, D. Wuebbles, and J.-J. Morcrette, 1990: Radiative forcing of climate. *Climate Change: The*

IPCC Scientific Assessment, J. Houghton, G. J. Jenkins, and J. J. Ephraums, Eds., Cambridge University Press, 41–68.

——, J. Cook, E. J. Highwood, and M. M. Joshi, 2003: An alternative to radiative forcing for estimating the relative importance of climate change mechanisms. *Geophys. Res. Lett.*, **30**, 2047, doi:10.1029/2003GL018141.

Smith, R. S., R. Sutton, and J. M. Gregory, 2014: The impact of salinity perturbations on the future uptake of heat by the Atlantic Ocean. *Geophys. Res. Lett.*, **41**, 9072–9079, doi:10.1002/2014GL062169.

Staten, P. W., T. Reichler, and J. Lu, 2014: The transient circulation response to radiative forcings and sea surface warming. *J. Climate*, **27**, 9323–9336, doi:10.1175/JCLI-D-14-00035.1.

Tomassini, L., and Coauthors, 2013: The respective roles of surface temperature driven feedbacks and tropospheric adjustment to CO_2 in CMIP5 transient climate simulations. *Climate Dyn.*, **41**, 3103–3126, doi:10.1007/s00382-013-1682-3.

Vial, J., J.-L. Dufresne, and S. Bony, 2013: On the interpretation of inter-model spread in CMIP5 climate sensitivity estimates. *Climate Dyn.*, **41**, 3339–3362, doi:10.1007/s00382-013-1725-9.

Watanabe, M., H. Shiogama, M. Yoshimori, T. Ogura, T. Yokohata, H. Okamoto, S. Emori, and M. Kimoto, 2012: Fast and slow timescales in the tropical low-cloud response to increasing CO_2 in two climate models. *Climate Dyn.*, **39**, 1627–1641, doi:10.1007/s00382-011-1178-y.

Webb, M., F. Lambert, and J. Gregory, 2013: Origins of differences in climate sensitivity, forcing and feedback in climate models. *Climate Dyn.*, **40**, 677–707, doi:10.1007/s00382-012-1336-x.

Williams, K. D., W. J. Ingram, and J. M. Gregory, 2008: Time variation of effective climate sensitivity in GCMs. *J. Climate*, **21**, 5076–5090, doi:10.1175/2008JCLI2371.1.

Winton, M., K. Takahashi, and I. Held, 2010: Importance of ocean heat uptake efficacy to transient climate change. *J. Climate*, **23**, 2333–2344, doi:10.1175/2009JCLI3139.1.

Wu, Y., R. Seager, M. Ting, N. Naik, and T. A. Shaw, 2012: Atmospheric circulation response to an instantaneous doubling of carbon dioxide. Part I: Model experiments and transient thermal response in the troposphere. *J. Climate*, **25**, 2862–2879, doi:10.1175/JCLI-D-11-00284.1.

Wyant, M. C., C. S. Bretherton, P. N. Blossey, and M. Khairoutdinov, 2012: Fast cloud adjustment to increasing CO_2 in a superparameterized climate model. *J. Adv. Model. Earth Syst.*, **4**, M05001, doi:10.1029/2011MS000092.

Zelinka, M. D., S. A. Klein, K. E. Taylor, T. Andrews, M. J. Webb, J. M. Gregory, and P. M. Forster, 2013: Contributions of different cloud types to feedbacks and rapid adjustments in CMIP5. *J. Climate*, **26**, 5007–5027, doi:10.1175/JCLI-D-12-00555.1.